

# Learning Gaussian Representation for Eye Fixation Prediction

Peipei Song

Data61/CSIRO, Australian National University  
Canberra, ACT 2601, Australia

Jing Zhang

Australian National University  
Canberra, ACT 2601, Australia

Piotr Koniusz

Data61/CSIRO, Australian National University  
Canberra, ACT 2601, Australia

Nick Barnes

Australian National University  
Canberra, ACT 2601, Australia

## Abstract

Existing eye fixation prediction methods perform the mapping from input images to the corresponding dense fixation maps generated from raw fixation points. However, due to the stochastic nature of human fixation, the generated dense fixation maps may be a less-than-ideal representation of human fixation. To provide a robust fixation model, we introduce “Gaussian Representation” for eye fixation modeling. Specifically, we propose to model the eye fixation map as a mixture of probability distributions, namely a Gaussian Mixture Model. In this new representation, we use several Gaussian distribution components as an alternative to the provided fixation map, which makes the model more robust to the randomness of fixation. Meanwhile, we design our framework upon some lightweight backbones to achieve real-time fixation prediction. Experimental results on three public fixation prediction datasets (SALICON, MIT1003, TORONTO) demonstrate that our method is fast and effective.

## 1. Introduction

While free viewing a specific scene, our eyes tend to focus on salient and informative regions that attract our attention. As a low-level image processing technique, saliency detection plays an important role in human visual recognition. Computer vision focuses on two main problems for saliency: eye fixation prediction and salient object detection. The former produces a heat map representing the degree of attention while the latter generates a salient segmentation map that highlights the entire scope of the salient object. As shown in Fig. 2, in contrast to salient object detection, fixation prediction is usually defined as a regression task that localizes the most discriminative region that

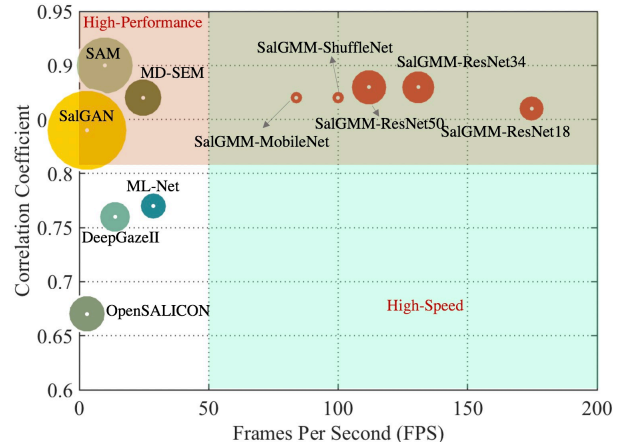


Figure 1. Comparison of state-of-the-art methods w.r.t. the number of model parameters, inference speed and the performance (correlation coefficient). The size of the circles indicates the number of model parameters. “SalGMM-\*” are several of our models where “\*” should be replaced by specific names of backbone networks.

attracts human attention.

The human visual system enjoys two kinds of attentional mechanisms: bottom-up [21, 16, 13, 8, 3, 53, 10] and top-down [44, 25, 26, 33, 34, 24, 6, 7, 5, 30, 17, 18, 9]. Bottom-up methods, also called feature driven methods, search for conspicuous regions in the image by computing contrast features, such as brightness, color, orientation, optical flow, *etc.* Top-down data-driven methods learn saliency from a large number of training examples [19] with clean labels. Such methods usually involve a deep convolutional neural network, which achieve fixation prediction by regression to a dense fixation map.

In the standard pipeline of the top-down models, the raw fixation points are blurred with a Gaussian filter to produce a dense fixation map serving as ground truth for fixation

prediction, where the fixation points are generally obtained by recording the fixation locations of multiple participants as they view the image. We observe that there exists a significant diversity in eye fixation patterns across individuals, as shown in Fig. 2. For images from the SALICON [19] dataset, we randomly select 70% of participants and then obtain the dense eye fixation map on the selected eye fixation points. With three random selections, we obtain three different fixation maps in Fig. 2.

The first example in Fig. 2 has two main focus points (the cat head and the laptop keyboard) as shown in the marked bounding boxes 1 and 2. The second example contains three regions of focus (the boy’s head, the woman’s head, and the pizza) as indicated by the marked bounding boxes 3, 4, and 5. While the three groups of participants agree on the main salient regions, the shape of the activation areas varies between individual participants. Meanwhile, there exist some isolated outliers (points outside of the boxes, particularly in columns 2 versus 3 and 4). This poses a question: “is reconstructing a per-pixel accurate fixation map the only way to model fixation prediction?”

As a regression task, the pixel-wise regression loss is usually used as a similarity measure for predicting the eye fixation maps, we argue that the randomness of the dense fixation map (as shown in Fig. 2) affects the generalization ability of the regression task, as fitting the isolated outliers may lead to unstable training. Therefore, we propose to model the dense fixation map with the Gaussian Mixture Model. In this way, instead of predicting a pixel-wise map, we operate in the parametric space of a distribution captured by the Gaussian Mixture Model (GMM) which represents a fixation map. We know that the process of annotation is subjective and thus the generated fixation maps are suboptimal from the statistical point of view due to variations in the behavior of different participants. In contrast, predicting parameters of a probability distribution requires fewer variables to predict which reduces overfitting. Thus, we learn a set of probability distributions rather than the fixation maps constructed from ground-truth fixation points.

Moreover, eye fixation prediction is usually defined as a pre-processing step for other computer vision-related fields, including video compression [12], object and action recognition [45, 35], *etc.* Therefore, the processing speed becomes a bottleneck for practical application use. In contrast, learning from a set of GMMs rather than dense fixation maps requires a relatively smaller network as shown in Fig. 1. Our model with ResNet18 [14] as the backbone (“SalGMM-ResNet18”) achieves comparable performance to the state-of-the-art model (MD-SEM [9]) while being seven times faster. We also show that employing lightweight backbones such as ShuffleNet [32] in our approach (“SalGMM-ShuffleNet”) leads to a network that is fast and small, and the obtained results are close to the state

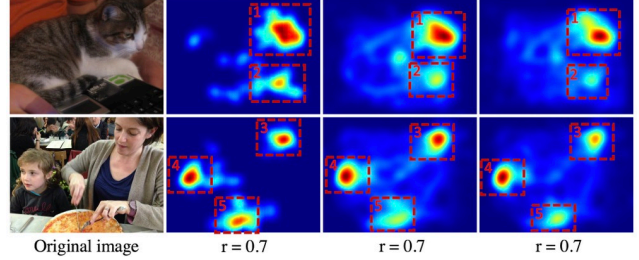


Figure 2. Dense fixation maps with different times of random selection. Param. “ $r=0.7$ ” indicates that we randomly sample 70% participants to generate the Gaussian blurred eye fixation map.

of the art. This potentially makes high-quality saliency prediction realistic on mobile devices [32] and edge devices [40].

To account for the randomness of labeling and provide an efficient eye fixation prediction model, we design an end-to-end neural network learning Gaussian Mixture Models, where dense fixation maps are represented as GMMs. To this end, a reconstruction loss is designed to learn the parameters of GMMs obtained from ground-truth eye fixation points. Our contributions are summarized as follows:

- i. We formulate the eye fixation map as a Gaussian Mixture Model. In contrast to existing methods, we employ a deep network to predict the parameters of a GMM instead of a dense saliency map per input image. For spatial locations, we express them w.r.t. the nearest reference centers represented by a spatial grid imposed over the spatial domain of images.
- ii. With the use of annotations for eye fixation, we design a novel reconstruction loss for learning the parameters of a GMM.
- iii. We perform ablation studies to investigate the impact of various backbones and spatial grid layouts and obtain real-time performing models as shown in Figure 1.
- iv. Experimental results on three benchmark fixation prediction datasets show both the effectiveness and efficiency of our solution.

## 2. Related Work

Below, we briefly introduce existing eye fixation prediction models and GMM-related eye fixation models.

**Bottom-Up Models.** Much research has been published on eye fixation prediction since the first paper [21] in 1985. Approach [42] proposed to model visual attention via selective tuning based on a hypothesis for primate visual attention. Following [42], Itti *et al.* [16] presented a visual attention system that combines multi-scale image features into a single topographical saliency map. This feature based model is robust to complex natural scenes. However, it cannot learn from new data because the model used hand-crafted features including color, intensity, and orientation.

As in approach [16], GBVS is a model consisting of two steps: forming an activation map on one feature map and normalizing them before combination [13]. CovSal [8] paid attention to integration by the use of correlation of image features as meta-features for saliency estimation. In [53], a novel saliency model based on a Boolean map was proposed. They used the concept of boolean map theory to characterize an image by a set of binary images. AIM [3] presented a novel visual saliency model on Information Maximization to explain the behaviors and reasons for certain components in visual saliency.

The aforementioned models are strong performers on various complex natural scenes because they have a simple architecture and are feature-based. In recent years, deep learning has become popular in computer vision. Deep models for eye fixation prediction significantly improve the performance compared with the traditional methods. Thus, we detail them below.

**Top-Down Models.** An early attempt at predicting saliency with a convnet was the ensemble of Deep Networks (eDN) [44]. This approach inspired DeepGaze I [25] to adopt a deeper network. In particular, DeepGaze I used the existing AlexNet network [23], where the fully connected layers were removed to keep the feature maps from the convolutional layers. The responses of each layer were fed into a linear model to learn weights. DeepGaze I is the first case of fine-tuning a convnet trained for classification whilst used for saliency. SalGAN adopts a second network discriminator to discriminate the output of a regular eye fixation generator with ground truth [33]. Approach [34] proposed two designs of network: a shallow convnet and a deep convnet, and formulated the eye fixation prediction as a minimization of the Euclidean distance of the predicted saliency map with the provided ground truth. This paper demonstrates that adversarial training improves the performance of saliency models. Approach [30] is a novel deep spatial contextual LSTM model. SAM [6] is also an LSTM based saliency attentive model that iteratively refines the predicted saliency map. Following SAM [6], MD-SEM [9] also adopted LSTM in their network to model the multiple duration saliency. ML-Net [5] combined features extracted at different levels of a Convolutional Neural Network (CNN) for eye fixation prediction. Approach [47] proposed an attentive salient network that learns the segmentation of salient objects from fixation maps under the assumption that salient object segmentation maps are fine-grained object-level representations of fixation maps. Approach [46] introduced a multi-scale eye fixation prediction model based on VGG-16 [39], with side outputs from lower levels fused together to achieve multi-scale eye fixation prediction. Approach [31] uses a multi-resolution CNN for predicting eye fixation. Each of these CNNs is trained to classify image patches as fixation-centered or non-fixation-

Dataset	Amount	Annotation	Viewers	Points	Resolution
SALICON[19]	20,000	mouse clicking	49-87	460	$480 \times 640$
MIT1003[20]	1003	eye tracking	15	66	Not fixed
TORONTO[2]	120	eye tracking	20	93	$511 \times 681$

Table 1. Summary of the eye fixation datasets.

centered. Approach [24] proposes a one-stream eye fixation framework with a location-biased convolutional layer to preserve center bias during the network training and two inception modules to obtain multi-scale representation.

Eye fixation prediction methods [17, 6] that formulate the eye fixation map as the probability distribution use a dedicated distribution-related loss. Approach [17] formulated an eye fixation map as a generalized Bernoulli distribution and then trained a deep model to predict such maps using novel loss functions. SAM [6] calculated the Correlation Coefficient and KL divergence as the loss functions.

**GMM-related Models.** A Gaussian Mixture Model is a probabilistic model based on a mixture of Gaussian distributions from observed data. For the classification problem, approach [43] directly estimated a GMM with a neural network to learn discriminative features by jointly optimizing the DNN feature layer and the GMM layer. Approach [54] proposed a patch-based model with shared latent variables from a GMM. For the eye fixation prediction, approach [6] only learns a set of center-bias prior maps generated with Gaussian functions. Several papers [48, 49, 37] used bottom-up hand-crafted features using the model [16], and modeled the corresponding eye fixation data using a GMM. In contrast to our approach, none of these models do not incorporate end-to-end learning of GMM features.

Approach [51] employed GMM to fit the gaze points from the predicted saliency map for scan path estimation. Method [11] estimated a GMM from the feature maps extracted from a bottom-up model referred to as Itti [16]. In contrast, our method learns to predict fixation maps in the parametric space of GMM from a given image by using CNN.

Our proposed approach is the first to use an end-to-end neural network to learn the parameters of a GMM to predict a probability distribution function over the image, that is the saliency map which predicts fixation.

### 3. Method

In this section, we first show that a fixation map can be represented by a 2D GMM with little error. We then explain how to use the neural network to learn a GMM with the supervision of eye fixation annotations.

#### 3.1. Fixation dataset analysis

While most eye fixation prediction datasets use eye tracking [20, 2] as shown in Table 1, the SALICON dataset

[19] validated mouse clicks as a model for eye fixation. The protocol based on mouse clicks enabled SALICON to be the largest eye fixation dataset. The original fixation ground truth contains the eye fixation points, as shown in Fig. 3(b). The dense fixation ground truth is composed by taking the aggregated fixation points from multiple viewers and applying a 2D Gaussian blur operation on the fixation points, as shown in Fig. 3(c). By analyzing multiple datasets, we find that fixation points fall around key image locations. For example, in Fig. 3(b), the fixation points are located on the dog, frisbee, and car. Therefore, the saliency map can be regarded as a Probability Density Function (PDF) of the saliency over spatial locations in the image, and it can be captured with the Gaussian Mixture Model.

### Fitting Eye Fixation Map via GMMs.

Firstly, we will analyze the possibility of using a GMM [38] to parameterize the eye fixation map. Let us take the SALICON dataset as an example. The fixation points are described as  $\mathbf{P} \equiv \{\mathbf{p}^k\}_{k=1}^N$ , where  $N$  is number of fixation points,  $k$  is an index over fixation points, and  $\mathbf{p}^k = (u^k, v^k)$  is the coordinate of the fixation point. In the standard fixation prediction pipeline [19], the ground truth fixation map  $\mathbf{I}_{gt}$  is obtained by applying a 2D Gaussian blur (for SALICON,  $\sigma = 19$ ) on  $\mathbf{P}$ . Instead of directly regressing w.r.t.  $\mathbf{I}_{gt}$ , we first obtain GMM on the fixation points with a parameter set  $\Theta \equiv \{(\pi^c, \mu_u^c, \mu_v^c, \sigma_u^c, \sigma_v^c, \sigma_{u,v}^c)\}_{c=1}^C$ , where  $\pi^c$  is the weight for each Gaussian component,  $\mu^c = (\mu_u^c, \mu_v^c)$  is the location of Gaussian component,  $\Sigma^c$  is the covariance matrix and  $c$  indexes the Gaussian components. The Gaussian covariance matrix is simply given as:

$$\Sigma^c = \begin{bmatrix} \sigma_u^c & \sigma_{u,v}^c \\ \sigma_{u,v}^c & \sigma_v^c \end{bmatrix}. \quad (1)$$

We then reconstruct one fixation map  $\mathbf{I}^c$  from the estimated component as:

$$\mathbf{I}^c \equiv \mathbf{I}(\mathbf{p}; \mu^c, \Sigma^c) = \frac{1}{2\pi\sqrt{|\Sigma^c|}} e^{-\frac{1}{2}(\mathbf{p}-\mu^c)^T \Sigma^{c-1} (\mathbf{p}-\mu^c)}, \quad (2)$$

where  $\mathbf{p}$  is the coordinate of fixation point. With multiple Gaussian components, we obtain the reconstructed fixation map  $\mathbf{I} = \sum_{c=1}^C \pi^c \mathbf{I}^c$  (we drop parameters for brevity).

Below, we set a different number of Gaussian components to fit the fixation points. Fig. 3(d)-(h) illustrates the reconstructed fixation map obtained by  $C$  Gaussian components. Fig. 3 shows that the reconstructed fixation map with  $C = 3$  has three separate focus locations on dog, frisbee, and car. When using more Gaussians, e.g.  $C = 5$ , to fit the fixation points, some Gaussian components may overlap with each other to fit the shape of fixation points. This observation motivates us to use relatively larger numbers of Gaussian components to obtain a better representation.

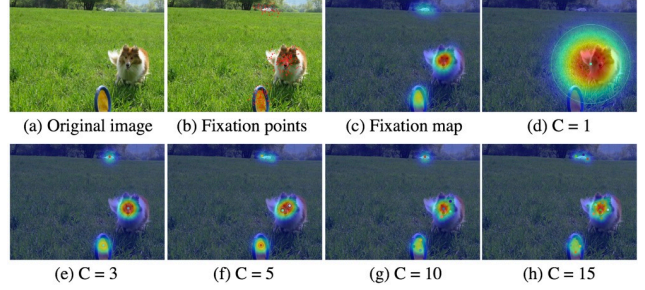


Figure 3. Visualization of the image, annotations, and GMM fitted fixation maps. Fixation map (c) is the Gaussian blurred eye fixation map. Figures (d)-(h) show the reconstructed fixation map given a different number of Gaussian components  $C$ . The solid circle and radius of the outer circle are the mean and standard deviation of the fitted Gaussian distribution.

Finally, we compare the reconstructed eye fixation map  $\mathbf{I}$  with the ground truth dense fixation map  $\mathbf{I}_{gt}$ . For the number of Gaussian components set to 20, we obtain Mean Squared Error (MSE), Kullback-Leibler divergence (KL), Correlation Coefficient (CC), Similarity (SIM), and Normalized Scanpath Saliency (NSS) equal to 0.0016, 0.0783, 0.9809, 0.8704, 2.3530 respectively. This shows that a GMM can be used to parameterize the eye fixation map with little error.

Thus, a saliency map can be modeled as a GMM over the image space. Rather than using a neural network to model the PDF directly by learning an image map using regression, in this paper, we directly output parameters of a GMM from our neural network.

## 3.2. Our proposed network-SalGMM

Section 3.1 demonstrated that it is possible to use a GMM in place of a dense eye fixation map. In this section, we build a neural network to learn a GMM for eye fixation prediction, as shown in Fig. 4. Our network includes three main parts: the ‘‘Feature Net’’, ‘‘Parameter Transformation’’, and ‘‘Reconstruction Loss’’.

### 3.2.1 Feature Net

As models that are fine-tuned on the ImageNet [23] perform better than those that are trained from scratch, we adopt commonly used feature extraction networks as the backbone. Following the backbone network, the ‘‘Gaussian Prediction Net’’ in Fig. 4 estimates the parameters of GMM. We only use ‘‘Pooling’’ and ‘‘Convolutional’’ layers in the Gaussian Prediction Net to preserve spatial information. In the Gaussian Prediction Net, we combine multi-scale features by using a similar architecture to FPN [28]. The outputs of Feature Net is a  $H \times W \times K$  dimensional feature map, where each  $K$  dimensional vector inside the feature map represents one Gaussian component



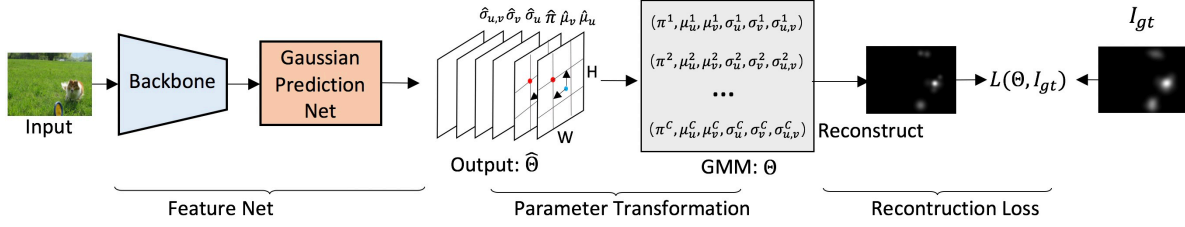


Figure 4. Network architecture. Note that centers of Gaussians are expressed w.r.t. the spatial reference grid.

( $K = 6$ ), as shown in Fig. 4. The number of components  $C = H \times W$  which coincides with the spatial size of feature maps. In this paper, we investigate 3 down-sampling scales: 32, 64 and 128. The outputs of the 3 scales are 16, 36, and 64 Gaussian components, respectively. We will show in the experimental results section that the number of Gaussian components is sufficient for our problem at hand. The output  $\hat{\Theta} \in \mathbb{R}^{H \times W \times K}$  represents a Gaussian component, and we define one Gaussian component as  $\hat{\theta}^c \equiv (\hat{\pi}^c, \hat{\mu}_u^c, \hat{\mu}_v^c, \hat{\sigma}_u^c, \hat{\sigma}_v^c, \hat{\sigma}_{u,v}^c)$ , where  $c \in \{1, \dots, C\}$ .

### 3.2.2 Parameter Transformation

Despite the output of the proposed network is  $\hat{\Theta}$ , due to the last layer of the ‘‘Gaussian Prediction Net’’ being a convolutional layer,  $\hat{\Theta}$  is not the actual set of GMM parameters that we use to represent the eye fixation map. Inspired by Faster R-CNN [36], we introduce a parameter transformation between the network output  $\hat{\Theta}$  and the actual GMM parameters  $\Theta$ . Faster R-CNN pre-computes multiple spatial anchor boxes w.r.t. the image and uses a neural network to regress the offsets from the anchor box to a nearby ground-truth box. In this paper, to predict a Gaussian component, we regress offsets between the anchor Gaussian centers (reference points) and the ground-truth Gaussian centers. Firstly, we use the ‘‘Sigmoid’’ activation function to scale the coordinate  $(\hat{\mu}_u^c, \hat{\mu}_v^c)$  from the output  $\hat{\Theta}$ . For example, as illustrated in Fig. 5 (a) for a  $3 \times 3$  output map, the estimated  $(\hat{\mu}_u^c, \hat{\mu}_v^c)$  is the offset to the nearby anchor point  $(u_a^c, v_a^c)$ . The grid size, or the scale of down-sampling in each dimension, is  $(w_a, h_a)$ . The actual locations of the GMMs are then computed as:

$$\mu_u^c = (\hat{\mu}_u^c + u_a^c) \cdot w_a \text{ and } \mu_v^c = (\hat{\mu}_v^c + v_a^c) \cdot h_a. \quad (3)$$

In a GMM, all of the  $\pi^c$  meet the constraint  $\sum_{c=1}^C \pi^c = 1$ , thus we use a ‘‘Softmax’’ layer as the activation function for  $\hat{\pi}^c$ . The weight  $\pi^c = \text{Softmax}(\hat{\pi}^c)$ , and the covariance  $(\sigma_u^c, \sigma_v^c, \sigma_{u,v}^c)$  do not require normalization.

### 3.2.3 Reconstruction Loss

Given the transformed GMM parameters  $\Theta$ , we reconstruct the fixation map  $\hat{I}$  before we compute the loss function.

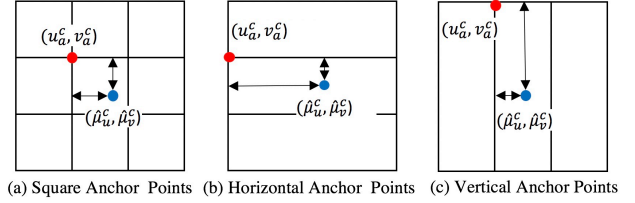


Figure 5. Three kinds of anchor settings (reference points).

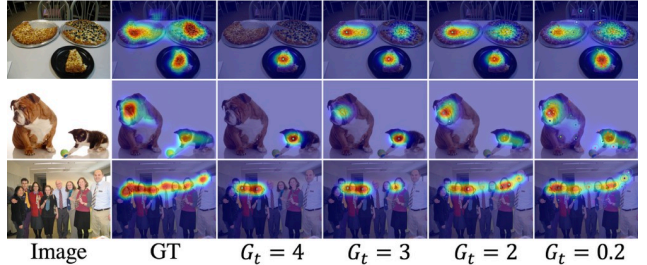


Figure 6. Visualization of predictions given different thresholds on the SALICON validation dataset.

We show the pipeline of our method in Algorithm 1. The reconstructed saliency map is formulated as:

$$\hat{I} = GMM(\Theta \mid \pi^c > G_t/C), c = \{1, \dots, C\}, \quad (4)$$

where  $G_t$  is the threshold for selecting Gaussian components. Fig. 6 shows reconstruction maps using different thresholds  $G_t$ . Our experimental results show that large  $G_t$  leads to efficient training and worse performance. The smaller  $G_t$ , on the contrary, benefits network performance while leading to longer training time. We set  $G_t = 0.2$  in our experiments to achieve a trade-off between network performance and training efficiency.

We define our loss function between the reconstructed saliency map  $\hat{I}$  and the eye fixation annotation  $I_{gt}$  as:

$$L(\Theta, I_{gt}) = \frac{\sigma(I_{gt}, GMM(\Theta \mid \pi^c > G_t/C))}{\sigma(I_{gt}) \cdot \sigma(GMM(\Theta \mid \pi^c > G_t/C))}, \quad (5)$$

where  $\sigma(\cdot)$  evaluates correlation. The correlation coefficient loss is also used in [6] but in a very different context. As we reconstruct  $\hat{I}$  by  $\Theta$ , the loss will learn parameters of GMM.

### Algorithm 1 Learning GMM Features for Predicting Eye Fixation

**Input:** Training images  $D = \{\mathbf{X}_i, \mathbf{I}_i, \mathbf{P}_i\}_{i=1}^{N_b}$ , where  $\mathbf{X}_i$ ,  $\mathbf{I}_i$  and  $\mathbf{P}_i$  are input RGB image, its dense fixation map and fixation points map.

**Output:** Parametric Gaussian Mixture Model  $\hat{\Theta} \equiv \{\hat{\Theta}_i\}_{i=1}^{N_b}$ . For each input image  $\mathbf{X}_i$ , the output is  $\hat{\Theta}_i$ , where  $C$  is the number of Gaussian components.

**Network Setup:** Maximum epoch is  $N_e$ , number of batches is  $N_b$  and learning rate is  $\gamma$ .  $F$  is the network.

- 1: **Step 1.** Initialize the backbone with the parameters pretrained on ImageNet.
- 2: **Step 2.** Train the network.
- 3: **for**  $t = 1, \dots, N_e$  **do**
- 4:     **for**  $i = 1, \dots, N_b$  **do**
- 5:         Compute the output of the network:  $\hat{\Theta}_i = F(\mathbf{X}_i)$ .
- 6:         Transform relative coord. to absolute:  $\hat{\Theta}_i \rightarrow \Theta_i$ .
- 7:         Reconstruct eye fixation map  $\hat{\mathbf{I}}_i$  by using  $\Theta_i$  (Eq. 4).
- 8:         Compute loss according to Eq. 5.
- 9:         Backprop. to update network parameters/learn GMM.
- 10:     **end for**
- 11: **end for**

## 4. Experimental Results

### 4.1. Experimental Setup

**Datasets:** **SALICON** [19] contains 10,000 training images, 5,000 validation images and 5,000 testing images, which are selected from the Microsoft COCO dataset [29]. The annotations are represented by mouse-clicking instead of eye tracking. We train our model on the SALICON training and validation sets and test on the SALICON test set, **MIT1003** dataset [20] and **TORONTO** dataset [2]. MIT1003 contains 1,003 images from Flickr and LabelMe, and the TORONTO dataset has 120 color images from indoor and outdoor scenes, as listed in Table. 1.

**Training Procedures:** Except where specified, we use ResNet pre-trained on ImageNet as the network backbone. We use two Geforce RTX 2080ti GPUs for training. We freeze the first two ResNet blocks and train the other parameters for 20 epochs with the learning rate  $10^{-3}$ . The training images are resized to  $352 \times 352$ . When testing, the images are also resized to  $352 \times 352$ .

**Evaluation Metrics:** The standard evaluation metrics are introduced by [4], including Pearson’s Correlation Coefficient (CC), Similarity (SIM), Kullback-Leibler divergence (KL), Earth Mover’s Distance (EMD), Normalized Scanpath Saliency (NSS), Area Under Curve (AUC), Information Gain (IG). Three variants for AUC: **AUC-Judd** [52], **AUC-Borji** [1] and shuffled AUC (**sAUC**) [1] are commonly used for evaluation. Evaluation metrics for eye fixation prediction are divided into two groups according to two kinds of annotations: Distribution-based metrics and

Methods	Distribution-based			Location-based			
	CC $\uparrow$	SIM $\uparrow$	KL $\downarrow$	NSS $\uparrow$	sAUC $\uparrow$	IG $\uparrow$	AUC-B $\uparrow$
Itti[16]	0.549	0.543	0.712	1.098	0.629	-0.005	0.773
GBVS[13]	0.639	0.585	0.598	1.262	0.612	0.172	0.807
OpenSALICON[41]	0.657	0.600	0.581	1.553	0.716	0.331	0.807
ML-NET[5]	0.762	0.668	0.639	1.802	0.723	0.461	0.838
SalNet[34]	0.622	-	-	1.859	0.724	-	0.858
DeepGazeII[27]	0.762	0.672	0.752	1.742	0.692	0.371	0.845
DeepFix[24]	0.804	-	-	-	0.630	0.315	0.761
SalGAN[33]	0.842	0.728	0.426	1.817	0.733	0.650	0.857
SAM-Res(17)[6]	0.899	0.793	0.611	1.990	0.741	0.538	0.865
EML-NET[18]	0.886	0.780	0.520	2.050	0.746	0.736	0.866
MD-SEM[9]	0.868	0.774	0.568	2.058	0.745	0.598	0.864
SalGMM	0.883	0.777	0.463	1.898	0.732	0.603	0.861

Table 2. Comparison results on the SALICON Saliency Prediction Challenge (LSUN 2017) testset.

Methods	Distribution-based				Location-based				
	CC $\uparrow$	SIM $\uparrow$	KL $\downarrow$	EMD $\downarrow$	NSS $\uparrow$	sAUC $\uparrow$	IG $\uparrow$	AUC-J $\uparrow$	AUC-B $\uparrow$
Itti [16]	0.33	0.32	1.48	5.18	1.10	0.64	0.23	0.78	0.76
GBVS [13]	0.42	0.36	1.30	4.34	1.38	0.63	0.27	0.83	0.82
AIM [3]	0.26	0.27	-	-	0.82	0.68	-	0.79	0.76
Judd Model[20]	0.30	0.29	-	-	1.02	0.68	-	0.76	0.74
CAS [10]	0.31	0.32	-	-	1.07	0.68	-	0.76	0.74
BMS [53]	0.36	0.33	1.46	5.33	1.25	0.69	0.25	0.79	0.76
eDN [44]	0.41	0.30	1.55	5.32	1.29	0.66	0.07	0.85	0.84
Mr-CNN [31]	0.38	0.35	-	-	1.36	0.73	-	0.80	0.77
ML-Net[5]	0.60	0.48	1.06	3.50	2.28	0.72	0.78	0.86	0.80
DVA [46]	0.64	0.50	0.95	3.89	2.38	0.72	0.85	0.88	0.81
DeepGazeII[27]	0.71	0.57	1.06	2.48	2.86	0.71	0.76	0.90	0.79
SalGAN [33]	0.63	0.51	1.00	3.21	2.21	0.74	0.68	0.88	0.85
SAM-Res(17)[6]	0.66	0.53	1.23	2.94	2.36	0.75	0.37	0.89	0.86
MD-SEM [9]	0.66	0.53	1.23	1.13	2.51	0.74	0.98	0.90	0.84
SalGMM	0.64	0.51	1.09	1.17	2.26	0.74	0.52	0.89	0.86

Table 3. Comparison results on the MIT1003 dataset.

Methods	Distribution-based				Location-based				
	CC $\uparrow$	SIM $\uparrow$	KL $\downarrow$	EMD $\downarrow$	NSS $\uparrow$	sAUC $\uparrow$	IG $\uparrow$	AUC-J $\uparrow$	AUC-B $\uparrow$
Itti[16]	0.48	0.48	0.97	2.88	1.30	0.66	0.32	0.80	0.79
GBVS[13]	0.57	0.49	0.85	2.29	1.52	0.64	0.31	0.83	0.82
AIM[3]	0.30	0.36	-	-	0.84	0.67	-	0.76	0.75
Judd[20]	0.41	0.40	-	-	1.15	0.67	-	0.78	0.77
CAS[10]	0.45	0.44	-	-	1.27	0.69	-	0.78	0.78
CovSal[8]	0.56	0.52	1.23	2.09	1.49	0.53	-0.15	0.82	0.77
BMS[53]	0.52	0.45	0.98	3.11	1.52	0.71	0.41	0.80	0.78
eDN[44]	0.50	0.40	1.12	3.06	1.25	0.62	0.12	0.85	0.84
Mr-CNN[31]	0.49	0.47	-	-	1.41	0.71	-	0.80	0.79
ML-Net[5]	0.65	0.56	1.12	2.07	2.00	0.69	0.20	0.85	0.76
DVA[46]	0.72	0.58	0.65	2.18	2.12	0.69	0.66	0.86	0.78
DeepGazeII[27]	0.77	0.65	1.01	1.48	2.26	0.69	0.21	0.88	0.79
SalGAN[33]	0.72	0.61	0.95	1.80	2.02	0.72	0.27	0.86	0.82
SAM-Res(17)[6]	0.74	0.62	1.86	1.76	2.14	0.72	0.60	0.86	0.82
MD-SEM [9]	0.70	0.61	1.82	1.75	2.12	0.70	0.72	0.86	0.78
SalGMM	0.73	0.61	0.77	1.74	2.06	0.72	0.69	0.87	0.83

Table 4. Comparison results on the TORONTO dataset.

Location-based metrics. The blurred fixation map is treated as a probability distribution. The metrics defined on the blurred fixation map are “Distribution based”, including CC, SIM, KL, and EMD. Similarly, the metrics defined on the fixation points are “Location-based”, namely NSS, sAUC, IG, AUC-Borji and AUC-Judd. We compare our proposed model with the competing methods on the two groups of metrics in Section 4.2.

Methods	Distribution-based				Location-based				Model Size		
	CC↑	SIM↑	KL↓	EMD↓	NSS↑	sAUC↑	IG↑	AUC-J↑	AUC-B↑	Params(M)	FPS
ML-Net[5]	0.766	0.671	0.567	1.345	1.779	0.674	0.575	0.846	0.740	15.5	28.6
DeepGazeII[27]	0.760	0.673	0.666	1.440	1.703	0.646	0.486	0.854	0.736	20.4	13.9
OpenSALICON[41]	0.666	0.600	0.562	1.762	1.543	0.692	0.406	0.814	0.758	29.4	3.0
SalGAN[33]	0.841	0.725	0.358	1.199	1.786	0.723	0.782	0.859	0.823	536.5	3.0
SAM(2017)[6]	0.900	0.794	0.495	0.864	1.959	0.728	0.694	0.869	0.829	70.1	9.9
MD-SEM [9]	0.873	0.778	0.536	0.870	2.025	0.702	0.722	0.870	0.784	30.9	24.7
Down sampling Scales											
ResNet50_D32_S_AS	0.884	0.765	0.276	0.992	1.880	0.723	0.862	0.866	0.832	26.7	106.6
ResNet50_D64_S_AS	0.880	0.769	0.371	0.950	1.861	0.725	0.858	0.863	0.833	26.7	111.9
ResNet50_D128_S_AS	0.837	0.734	0.527	1.048	1.736	0.703	0.709	0.850	0.817	26.7	111.5
Gaussian Covariance											
ResNet50_D64_D_AS	0.881	0.771	0.365	0.951	1.862	0.728	0.864	0.864	0.837	26.7	109.2
ResNet50_D64_F_AS	0.873	0.725	0.339	1.290	1.832	0.719	0.728	0.862	0.836	26.7	108.5
Anchor Settings											
ResNet50_D64_S_AN	0.854	0.746	0.354	1.014	1.793	0.713	0.790	0.857	0.823	26.7	111.9
ResNet50_D64_S_AH	0.841	0.732	0.347	1.069	1.748	0.703	0.743	0.854	0.819	26.7	111.9
ResNet50_D64_S_AV	0.834	0.718	0.350	1.112	1.719	0.698	0.688	0.850	0.821	26.7	111.9
Backbone Networks											
ResNet34_D64_S_AS	0.877	0.767	0.364	0.959	1.850	0.724	0.851	0.863	0.833	23.6	131.0
ResNet18_D64_S_AS	0.864	0.756	0.392	1.014	1.821	0.720	0.819	0.860	0.829	13.5	174.8
MobileNetv3_D64_S_AS	0.869	0.754	0.347	1.025	1.832	0.716	0.812	0.860	0.826	4.0	83.8
ShuffleNetv2_D64_S_AS	0.867	0.751	0.297	1.038	1.820	0.718	0.811	0.861	0.831	3.9	99.9

Table 5. Ablation study on the SALICON validation set. The notation of method names follows “Backbone.Scale.Gaussian Covariance.Grid Map”, down-sampled predictions by 32, 64 and 128 $\times$  are “\_D32”, “\_D64” and “\_D128”. We evaluate the use of isotropic Gaussians, on-diagonal variances only, and full covariances: (i) “\_S” ( $\sigma_u = \sigma_v$ ,  $\sigma_{u,v} = 0$ ), (ii) “\_D” ( $\sigma_{u,v} = 0$ ) and (iii) “\_F” ( $\sigma_{u,v}$ ,  $\sigma_u$ ,  $\sigma_v$ ). We also evaluate “Anchor Settings”, including square grid (AS), horizontal-only grid (AH), vertical-only grid (AV), and none (AN).

## 4.2. Performance evaluation

**Quantitative Evaluation.** We compare the proposed network with competing methods on three publicly available datasets and show the performance in Table 2, Table 3 and Table 4 respectively. The code and models of several competing methods are available online, including Itti<sup>1</sup> and GBVS<sup>1</sup>, OpenSALICON<sup>2</sup>, ML-Net<sup>3</sup>, SalGAN<sup>4</sup>, DeepGazeII<sup>5</sup>, SAM<sup>6</sup> and MD-SEM<sup>7</sup>. We list nine evaluation metrics in these three tables. Our model SalGMM (ResNet50\_D64\_S\_AS in Table. 2) uses ResNet50 as the backbone. “red” indicates the best performance, “green” is the second best and “blue” is the third best. Comparing our performance with competing methods in all these three benchmark testing datasets, we observe that our model (“SalGMM”) ranks in the top three on most metrics.

**Qualitative Evaluation.** Fig. 7 shows several samples from the SALICON validation set on multiple competing methods, including Itti [16], OpenSALICON [41], DeepGazeII [27], SalGAN [33], ML-Net [5], SAM [6], MD-SEM [9]. Itti is a hand-crafted method, while the others are deep models. Fig. 7 shows that our model predicts a similar map compared to SAM and MD-SEM. However, our model performs better at locating the peak response of object regions.

**Runtime and Model Size Comparison.** We implement our

GMM representation based eye fixation prediction model with multiple backbone networks as shown in Table. 5, including ResNet (ResNet50, ResNet34, ResNet18) [14], MobileNet-v3 [15] and ShuffleNet-v2 [32]. The reported performance “SalGMM” in Table 2, Table 3 and Table 4 corresponds to “ResNet50\_D64\_S\_AS” in Table 5. We observe the competing performance of our models compared with state-of-the-art models. Meanwhile, the smaller model size and higher frame/second rate further indicate both effectiveness and efficiency of our proposed solution.

We further show the inference time of six benchmark eye fixation models (ML-Net [5], DeepGazeII [26], SAM [6], OpenSalicon [41], SalGAN [33] and MD-SEM [9]) and our models in Fig. 1. The figure shows that all the competing methods have much longer inference time than ours. Meanwhile, the size of the circle indicates the size of the model. Our ShuffleNet and MobileNet based models have very small model sizes and comparable performance to the state-of-the-art methods. Although ML-Net and DeepGazeII are smaller in model size than our ResNet50 and ResNet34 based models, the big gap in inference time further demonstrates the efficiency of our solution.

## 4.3. Ablation Study

We carried out the following ablation study to thoroughly analyze the proposed framework.

**Down Sampling Scales.** As mentioned in Section 3.2, we test 3 different scales of the down-sampling step. The sub-block “Down sampling scales” in Table 5 shows the performance on the SALICON validation set with the three different scales of down-sampling. The better performance of

<sup>1</sup><http://www.klab.caltech.edu/harel/share/gbvs.php>

<sup>2</sup><https://github.com/CLT29/OpenSALICON>

<sup>3</sup><https://github.com/marcellacornia/mlnet>

<sup>4</sup><https://github.com/imatge-upc/salgan>

<sup>5</sup><https://deepgaze.bethgelab.org>

<sup>6</sup><https://github.com/marcellacornia/sam>

<sup>7</sup><http://multiduration-saliency.csail.mit.edu>



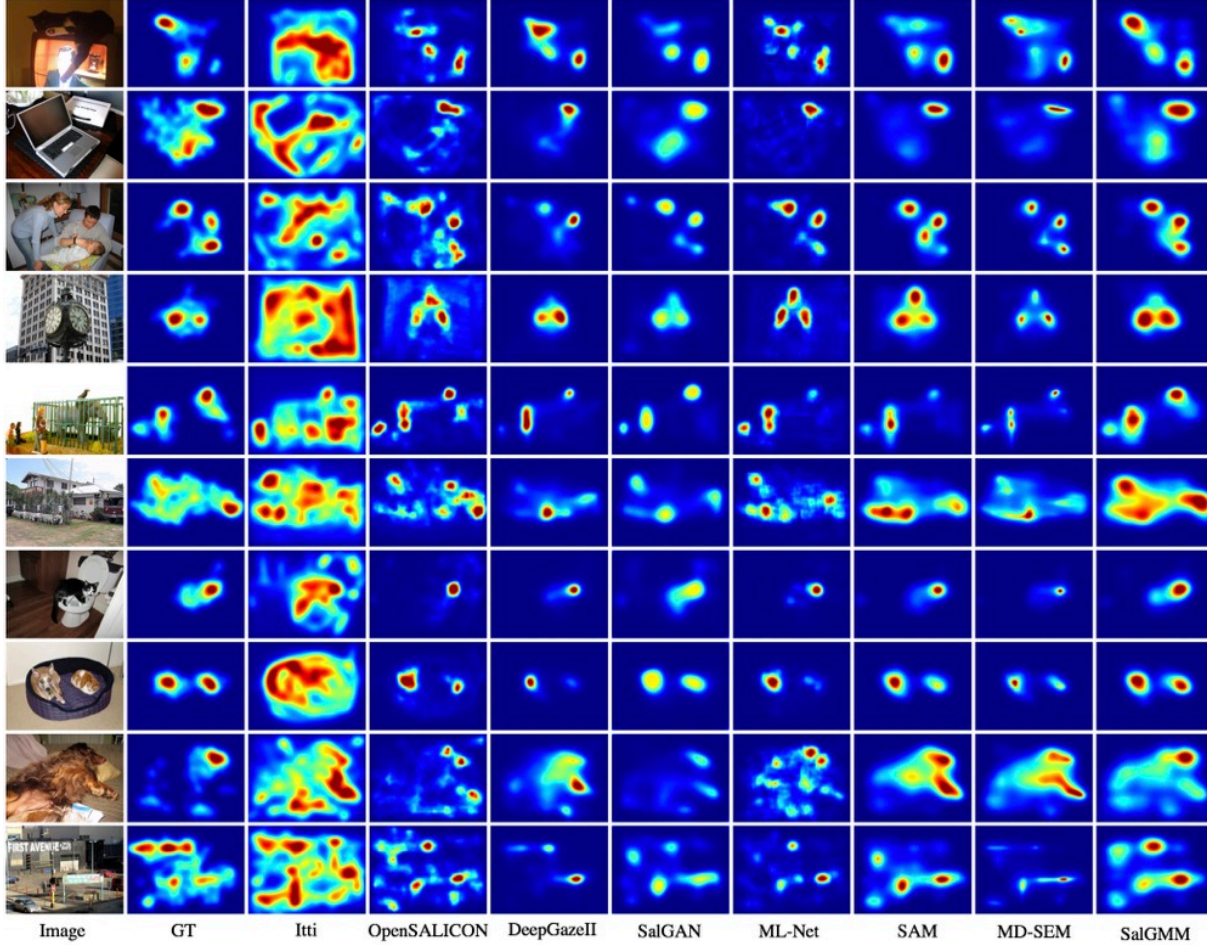


Figure 7. Comparison of predictions for our method versus competing methods on the SALICON validation set.

“ResNet50\_D32\_S\_AS” and “ResNet50\_D64\_S\_AS” compared with “ResNet50\_D128\_S\_AS” indicates that less down-sampling works better in our scenario.

**Gaussian Covariance.** We evaluate three modes of Gaussian covariance: “Spherical”, “Diag” and “Full”. “Spherical” represents an isotropic Gaussian. The level sets of “Spherical” Gaussian distribution are circles. For the “Diag” Gaussian distribution, the two elements  $u$  and  $v$  are independent. For the “Full” Gaussian distribution,  $u$  and  $v$  are correlated. The level sets of “Full” and “Diag” Gaussian distributions are ellipses. Table. 5 shows the performance of the three types of Gaussian modes in the sub-block “Gaussian covariance”. The overall performance of “Diag” Gaussian distribution works better than the “Full” Gaussian distribution.

**Anchor Settings.** In Fig. 5, we show three anchor settings. The neural network computes the coordinate offsets from the anchor point (marked as red points) to the ground-truth point rather than the location itself. The square grid is utilized in object detection networks [36]. We use both the horizontal grid and vertical grid map which is a popu-

lar practice in bag-of-words [50, 22]. We observe that the square grid-based model (“ResNet50\_D64\_S\_AS”) outperforms the other “horizontal only”, “vertical only” and “no grid” map, which indicates the square grid map works best in our task.

**Backbone Networks.** As discussed before, we evaluate our solution for multiple backbone networks, including ResNet (ResNet50, ResNet34, ResNet18) [14], MobileNet-v3 [15] and ShuffleNet-v2 [32], and show the performance in Table 5. The smaller size of MobileNet-v3 and ShuffleNet-v2 based models allows our solution to be effectively applied on mobile devices.

## 5. Conclusions

In this paper, we formulate the eye fixation prediction as learning of parameters of Gaussian Mixture Model. Our model generates 216 output variables ( $H \times W \times K$ ) whereas deep models that estimate a dense saliency map output 123,904 output variables with an input size of  $352 \times 352$ . For the model size, learning a GMM instead of a dense saliency map requires a relatively small number of network



parameters, *e.g.*, the parameters number of the model with ShuffleNet-v2 and MobileNet-v3 as backbones are 4M and 3.9M respectively. The new formulation of eye fixation also greatly decreases the inference time. We can reach a processing speed of 174.8 FPS, which indicates that our method works in real-time. Further, we show that our approach leads to a smaller network with competitive performance, which makes it suitable for embedded devices. To the best of our knowledge, this paper is the first to formulate an eye fixation prediction task as GMM parameter estimation. We evaluated the proposed method on three public datasets: SALICON, MIT1003, and TORONTO. The performance comparison, inference time comparison, and network size comparison demonstrate that our method is fast and effective.

## References

- [1] Ali Borji, Dicky N Sihite, and Laurent Itti. Quantitative analysis of human-model agreement in visual saliency modeling: A comparative study. *IEEE Transactions on Image Processing*, 22(1):55–69, 2012.
- [2] Neil Bruce and John Tsotsos. Attention based on information maximization. *Journal of Vision*, 7(9):950–950, 2007.
- [3] Neil DB Bruce and John K Tsotsos. Saliency, attention, and visual search: An information theoretic approach. *Journal of vision*, 9(3):5–5, 2009.
- [4] Zoya Bylinskii, Tilke Judd, Aude Oliva, Antonio Torralba, and Frédo Durand. What do different evaluation metrics tell us about saliency models? *IEEE transactions on pattern analysis and machine intelligence*, 41(3):740–757, 2018.
- [5] Marcella Cornia, Lorenzo Baraldi, Giuseppe Serra, and Rita Cucchiara. A deep multi-level network for saliency prediction. In *2016 23rd International Conference on Pattern Recognition (ICPR)*, pages 3488–3493. IEEE, 2016.
- [6] Marcella Cornia, Lorenzo Baraldi, Giuseppe Serra, and Rita Cucchiara. Predicting human eye fixations via an lstm-based saliency attentive model. *IEEE Transactions on Image Processing*, 27(10):5142–5154, 2018.
- [7] Samuel F Dodge and Lina J Karam. Visual saliency prediction using a mixture of deep neural networks. *IEEE Transactions on Image Processing*, 27(8):4080–4090, 2018.
- [8] Erkut Erdem and Aykut Erdem. Visual saliency estimation by nonlinearly integrating features using region covariances. *Journal of vision*, 13(4):11–11, 2013.
- [9] Camilo Fosco, Anelise Newman, Pat Sukhum, Yun Bin Zhang, Nanxuan Zhao, Aude Oliva, and Zoya Bylinskii. How much time do you have? modeling multi-duration saliency. In *Proceedings of the IEEE/CVF Conference on Computer Vision and Pattern Recognition*, pages 4473–4482, 2020.
- [10] Stas Goferman, Lihi Zelnik-Manor, and Ayellet Tal. Context-aware saliency detection. *IEEE transactions on pattern analysis and machine intelligence*, 34(10):1915–1926, 2011.
- [11] Hairu Guo, Xiaojie Wang, Yixin Zhong, and Song Bi. An improved salbayes model with gmm. In *International Conference on Computer Analysis of Images and Patterns*, pages 356–363. Springer, 2011.
- [12] Hadi Hadizadeh and Ivan V Bajić. Saliency-aware video compression. *IEEE Transactions on Image Processing*, 23(1):19–33, 2013.
- [13] Jonathan Harel, Christof Koch, and Pietro Perona. Graph-based visual saliency. In *Advances in neural information processing systems*, pages 545–552, 2007.
- [14] Kaiming He, Xiangyu Zhang, Shaoqing Ren, and Jian Sun. Deep residual learning for image recognition. In *Proceedings of the IEEE conference on computer vision and pattern recognition*, pages 770–778, 2016.
- [15] Andrew Howard, Mark Sandler, Grace Chu, Liang-Chieh Chen, Bo Chen, Mingxing Tan, Weijun Wang, Yukun Zhu, Ruoming Pang, Vijay Vasudevan, et al. Searching for mobilenetv3. In *Proceedings of the IEEE International Conference on Computer Vision*, pages 1314–1324, 2019.
- [16] Laurent Itti, Christof Koch, and Ernst Niebur. A model of saliency-based visual attention for rapid scene analysis. *IEEE Transactions on Pattern Analysis & Machine Intelligence*, (11):1254–1259, 1998.
- [17] Saumya Jetley, Naila Murray, and Eleonora Vig. End-to-end saliency mapping via probability distribution prediction. In *Proceedings of the IEEE Conference on Computer Vision and Pattern Recognition*, pages 5753–5761, 2016.
- [18] Sen Jia and Neil DB Bruce. Eml-net: An expandable multi-layer network for saliency prediction. *Image and Vision Computing*, page 103887, 2020.
- [19] Ming Jiang, Shengsheng Huang, Juanyong Duan, and Qi Zhao. Salicon: Saliency in context. In *Proceedings of the IEEE conference on computer vision and pattern recognition*, pages 1072–1080, 2015.
- [20] Tilke Judd, Krista Ehinger, Frédo Durand, and Antonio Torralba. Learning to predict where humans look. In *2009 IEEE 12th international conference on computer vision*, pages 2106–2113. IEEE, 2009.
- [21] Christof Koch and Shimon Ullman. Shifts in selective visual attention: Towards the underlying neural circuitry. 4:219–27, 02 1985.
- [22] Piotr Koniusz, Fei Yan, Philippe-Henri Gosselin, and Kryszian Mikolajczyk. Higher-order occurrence pooling for bags-of-words: Visual concept detection. *IEEE transactions on pattern analysis and machine intelligence*, 39(2):313–326, 2016.
- [23] Alex Krizhevsky, Ilya Sutskever, and Geoffrey E Hinton. Imagenet classification with deep convolutional neural networks. In *Advances in neural information processing systems*, pages 1097–1105, 2012.
- [24] Srinivas SS Kruthiventi, Kumar Ayush, and R Venkatesh Babu. Deepfix: A fully convolutional neural network for predicting human eye fixations. *IEEE Transactions on Image Processing*, 26(9):4446–4456, 2017.
- [25] Matthias Kümmerer, Lucas Theis, and Matthias Bethge. Deep gaze i: Boosting saliency prediction with feature maps trained on imagenet. *arXiv preprint arXiv:1411.1045*, 2014.
- [26] Matthias Kümmerer, Thomas SA Wallis, and Matthias Bethge. Deepgaze ii: Reading fixations from deep

- features trained on object recognition. *arXiv preprint arXiv:1610.01563*, 2016.
- [27] Matthias Kummerer, Thomas SA Wallis, Leon A Gatys, and Matthias Bethge. Understanding low-and high-level contributions to fixation prediction. In *Proceedings of the IEEE International Conference on Computer Vision*, pages 4789–4798, 2017.
- [28] Tsung-Yi Lin, Piotr Dollár, Ross Girshick, Kaiming He, Bharath Hariharan, and Serge Belongie. Feature pyramid networks for object detection. In *Proceedings of the IEEE conference on computer vision and pattern recognition*, pages 2117–2125, 2017.
- [29] Tsung-Yi Lin, Michael Maire, Serge Belongie, James Hays, Pietro Perona, Deva Ramanan, Piotr Dollár, and C Lawrence Zitnick. Microsoft coco: Common objects in context. In *European conference on computer vision*, pages 740–755. Springer, 2014.
- [30] Nian Liu and Junwei Han. A deep spatial contextual long-term recurrent convolutional network for saliency detection. *IEEE Transactions on Image Processing*, 27(7):3264–3274, 2018.
- [31] Nian Liu, Junwei Han, Dingwen Zhang, Shifeng Wen, and Tianming Liu. Predicting eye fixations using convolutional neural networks. In *Proceedings of the IEEE Conference on Computer Vision and Pattern Recognition*, pages 362–370, 2015.
- [32] Ningning Ma, Xiangyu Zhang, Hai-Tao Zheng, and Jian Sun. Shufflenet v2: Practical guidelines for efficient cnn architecture design. In *Proceedings of the European conference on computer vision (ECCV)*, pages 116–131, 2018.
- [33] Junting Pan, Cristian Canton Ferrer, Kevin McGuinness, Noel E O’Connor, Jordi Torres, Elisa Sayrol, and Xavier Giro-i Nieto. Salgan: Visual saliency prediction with generative adversarial networks. *arXiv preprint arXiv:1701.01081*, 2017.
- [34] Junting Pan, Elisa Sayrol, Xavier Giro-i Nieto, Kevin McGuinness, and Noel E O’Connor. Shallow and deep convolutional networks for saliency prediction. In *Proceedings of the IEEE Conference on Computer Vision and Pattern Recognition*, pages 598–606, 2016.
- [35] Konstantinos Rapantzikos, Yannis Avrithis, and Stefanos Kollias. Dense saliency-based spatiotemporal feature points for action recognition. In *2009 IEEE Conference on Computer Vision and Pattern Recognition*, pages 1454–1461. Ieee, 2009.
- [36] Shaoqing Ren, Kaiming He, Ross Girshick, and Jian Sun. Faster r-cnn: Towards real-time object detection with region proposal networks. In *Advances in neural information processing systems*, pages 91–99, 2015.
- [37] Yun Ren, Zulin Wang, Mai Xu, Haoyu Dong, and Shengxi Li. Learning dynamic gmm for attention distribution on single-face videos. In *Proceedings of the IEEE Conference on Computer Vision and Pattern Recognition Workshops*, pages 29–38, 2017.
- [38] Douglas A Reynolds. Gaussian mixture models. *Encyclopedia of biometrics*, 741, 2009.
- [39] Karen Simonyan and Andrew Zisserman. Very deep convolutional networks for large-scale image recognition. *arXiv preprint arXiv:1409.1556*, 2014.
- [40] Sony. Sony’s first image sensor with AI processing, 2020. [www.youtube.com/watch?v=VycSn3xrMcA&feature=emb\\_title](https://www.youtube.com/watch?v=VycSn3xrMcA&feature=emb_title).
- [41] Christopher Lee Thomas. Opensalicon: An open source implementation of the salicon saliency model. Technical Report TR-2016-02, University of Pittsburgh, 2016.
- [42] John K Tsotsos, Scan M Culhane, Winky Yan Kei Wai, Yuzhong Lai, Neal Davis, and Fernando Nuflo. Modeling visual attention via selective tuning. *Artificial intelligence*, 78(1-2):507–545, 1995.
- [43] Ehsan Variani, Erik McDermott, and Georg Heigold. A gaussian mixture model layer jointly optimized with discriminative features within a deep neural network architecture. In *2015 IEEE International Conference on Acoustics, Speech and Signal Processing (ICASSP)*, pages 4270–4274. IEEE, 2015.
- [44] Eleonora Vig, Michael Dorr, and David Cox. Large-scale optimization of hierarchical features for saliency prediction in natural images. In *Proceedings of the IEEE Conference on Computer Vision and Pattern Recognition*, pages 2798–2805, 2014.
- [45] Dirk Walther, Laurent Itti, Maximilian Riesenhuber, Tomaso Poggio, and Christof Koch. Attentional selection for object recognition—a gentle way. In *International workshop on biologically motivated computer vision*, pages 472–479. Springer, 2002.
- [46] Wenguan Wang and Jianbing Shen. Deep visual attention prediction. *IEEE Transactions on Image Processing*, 27(5):2368–2378, 2017.
- [47] Wenguan Wang, Jianbing Shen, Xingping Dong, and Ali Borji. Salient object detection driven by fixation prediction. In *Proceedings of the IEEE Conference on Computer Vision and Pattern Recognition*, pages 1711–1720, 2018.
- [48] Mai Xu, Yun Ren, and Zulin Wang. Learning to predict saliency on face images. In *Proceedings of the IEEE International Conference on Computer Vision*, pages 3907–3915, 2015.
- [49] Mai Xu, Yun Ren, Zulin Wang, Jingxian Liu, and Xiaoming Tao. Saliency detection in face videos: A data-driven approach. *IEEE Transactions on Multimedia*, 20(6):1335–1349, 2017.
- [50] Jianchao Yang, Kai Yu, and Thomas Huang. Efficient highly over-complete sparse coding using a mixture model. In *European Conference on Computer Vision*, pages 113–126. Springer, 2010.
- [51] Ryo Yonetani, Hiroaki Kawashima, and Takashi Matsuyama. Multi-mode saliency dynamics model for analyzing gaze and attention. In *Proceedings of the Symposium on Eye Tracking Research and Applications*, pages 115–122, 2012.
- [52] T. Judd Z. Bylinskii, L. Itti A. Borji, A. Oliva F. Durand, and A. Torralba. Mit saliency benchmark (2014). [Online]. Available:<http://saliency.mit.edu>.
- [53] Jianming Zhang and Stan Sclaroff. Saliency detection: A boolean map approach. In *Proceedings of the IEEE international conference on computer vision*, pages 153–160, 2013.

- [54] Yingying Zhu, Youbao Tang, Yuxing Tang, Daniel C Elton, Sungwon Lee, Perry J Pickhardt, and Ronald M Summers. Cross-domain medical image translation by shared latent gaussian mixture model. *arXiv preprint arXiv:2007.07230*, 2020.